Available online at www.sciencedirect.com
ScienceDirect
Journal of Power Sources 172 (2007) 805–815
JOURNAL OF POWER SOURCES
www.elsevier.com/locate/jpowsour

A 3D model for the free-breathing direct methanol fuel cell: Methanol crossover aspects and validations with current distribution measurements

V. Saarinen [a,*], O. Himanen [b], T. Kallio [a], G. Sundholm [a], K. Kontturi [a]

[a] *Helsinki University of Technology, Laboratory of Physical Chemistry and Electrochemistry, P.O. Box 6100, 02015 TKK, Finland*
[b] *Helsinki University of Technology, Laboratory of Advanced Energy Systems, P.O. Box 2200, 02015 TKK, Finland*

Received 8 March 2007; received in revised form 19 April 2007; accepted 6 May 2007
Available online 18 May 2007

Abstract

A three-dimensional model has been developed for the free-breathing direct methanol fuel cell (DMFC) assuming steady-state isothermal and single-phase conditions. Especially the MeOH crossover phenomenon is investigated and the model validations are done using previous cathodic current distribution measurements. A free convection of air is modelled in the cathode channels and diffusion and convection of liquid (anode) and gaseous species (cathode) in the porous transport layers. The MeOH flow in the membrane is described with diffusion and protonic drag. The parameter ψ in the model describes the MeOH oxidation rate at the cathode and it is fitted according to the measured current distributions. The model describes the behaviour of the free-breathing DMFC, when different operating parameters such as cell temperature, MeOH concentration and flow rate are varied in a wide range. The model also predicts the existence of the experimentally observed electrolytic domains, i.e. local regions of negative current densities. Altogether, the developed model is in reasonable agreement with both the measured current distributions and polarization curves. The spatial information gained of mass transfer phenomena inside the DMFC is valuable for the optimization of the DMFC operating parameters.

Keywords: DMFC; Free-breathing; 3D model; Current distribution; Methanol crossover

1. Introduction

Conventional batteries are soon becoming inadequate for the increasing power requirements of portable electronic devices and computers [1]. The alternative power supply in the future could be the direct methanol fuel cell (DMFC). The DMFC is a polymer electrolyte fuel cell (PEFC), where the anode reactant is a liquid mixture of MeOH and water. The use of MeOH gives some advantages compared to the hydrogen systems: the storage of the fuel is easier and the refueling systems can have a simpler structure. Because of simplicity, space saving and economical reasons, some DMFC applications will probably be totally passive-feed DMFCs, free-breathing and without any external pumps.

In order to optimize performance values for the DMFC, it is important to have even current and temperature distributions inside the fuel cell. This can be achieved, when the concentrations of the reactants have optimum values. In many cases the goal of the fuel cell development is also to achieve an even current density profile under a variety of operating conditions. As a consequence, current distribution measurements are very valuable for the better understanding of the complex relationships between different variables and operating parameters of the DMFC. The current distribution measurements have been used in many PEFC [2–11] and DMFC [12–16] studies during recent years.

In the case of the DMFC, the MeOH crossover (MeOH permeability through the membrane) is a very dominating loss mechanism [17] and it has been investigated widely [18–29]. However, most of these studies have been performed without current distribution measurements. The MeOH permeating from anode to cathode poisons the Pt catalyst and causes mixed

* Corresponding author. Tel.: +358 50 5259669; fax: +358 94512580.
E-mail address: vss@cc.hut.fi (V. Saarinen).

0378-7753/$ – see front matter © 2007 Elsevier B.V. All rights reserved.
doi:10.1016/j.jpowsour.2007.05.029

Nomenclature

c	concentration (mol m^{-3} or M)
D	diffusion coefficient (m^2 s^{-1})
E	voltage (V)
F	Faraday's constant (96 485 C mol^{-1})
$\mathbf{g}$	acceleration due to gravity (9.81 m s^{-2})
i	current density (A m^{-2})
l	thickness (m)
M	molar mass (kg mol^{-1})
$\mathbf{N}$	molar flux (mol m^{-2} s^{-1})
p	pressure (Pa or atm)
R	universal gas constant (8.314 J mol^{-1} K^{-1})
RH	relative humidity (%)
T	temperature (K or °C)
$\mathbf{u}$	velocity (m s^{-1})
Σv	diffusion volume
$\dot{V}$	flow rate (m^3 s^{-1})
x	horizontal coordinate in the model (m)
X	mole fraction
y	vertical coordinate in the model (m)
z	coordinate perpendicular to xy-plane (m)

Subscripts and superscripts

0	reference
a	anode
amb	ambient
ave	average
c	cathode
cell	fuel cell
cr	critical
eff	effective
ele	electrode
i	species
j	species
liq	liquid
m	protonic phase
mem	membrane
ptl	porous transport layer
ref	reference
s	electronic phase

Greek letters

α	transfer coefficient of electrochemical reaction
ϵ	porosity
η	overpotential (V)
κ	intrinsic permeability (m^2)
λ	electro-osmotic drag coefficient
μ	dynamic viscosity (kg m^{-1} s^{-1})
ρ	density (kg m^{-3})
σ	conductivity (S m^{-1})
ϕ	potential (V)
ψ	parameter for MeOH oxidation rate at cathode (m s^{-1})

potentials, which decrease the fuel cell performance [30,31]. The polarization losses are caused mainly because MeOH is oxidized heterogeneously in the presence of oxygen [32]. Ye and Zhao [33] have observed a significant decline of open circuit voltage (OCV) in the DMFC, when the oxygen flow rate is reduced below a critical value. This can be explained with the coexistence of galvanic and electrolytic reactions in the DMFC, even when the cell is operated under open circuit conditions [34,35]. These reactions produce self-discharging currents in the DMFC causing MeOH consumption and H_2 evolution. On the contrary, when the oxygen flow rate is above a certain value, the OCV is observed to be very insensitive to this quantity [33]. For investigation of that kind of phenomena, the DMFC with a segmented cathode can be useful and provide detailed information on local concentrations of the reacting species, on which part of the DMFC most of the current is produced and how much the MeOH crossover phenomenon decreases the cell performance locally.

Many fuel cell models for the PEFC and the DMFC have been developed, see, e.g. review articles of Wang [36], Weber et al. [37] and Yao et al. [38], but most of the DMFC model validations have only been done using measured polarization curves, e.g. [38–44]. Models for passive-feed DMFCs with heat transfer effect have been set up by Chen and Zhao [45](1D) and Rice and Faghri [41](2D). Wang and Wang [43] have proposed a 2D two-phase model and Danilov et al. [44] a 3D two-phase model of a liquid-feed DMFC. Kjeang et al. [46] have published a 3D model of a flowing electrolyte DMFC to simulate MeOH crossover by convection and diffusion and Liu and Wang [47] a 3D two-phase DMFC model to investigate electron transport. Ge et al. [48] have made a 3D single-phase model of the DMFC to study the effects of MeOH crossover, porosities, MeOH flow rates and channel shoulder widths.

Ju et al. [49] have set up a 3D PEFC model (H_2 feed) and validated it with measured current distribution data. They also concluded that model validations against only polarization curves is insufficient and often misleading [49]. Because the chemical reactions and connections between different operational parameters in many cases are more complicated in the DMFC than in the hydrogen fed PEFC, there is a true need for DMFC model validations using current distribution data. However, this kind of 3D model for the free-breathing DMFC has not been reported so far. In this paper a 3D model for the free-breathing DMFC is presented and the model validations are done using our previously published current distribution measurements [12].

2. Modelling

2.1. General model description, geometry and assumptions

A three-dimensional model of the free-breathing direct methanol fuel cell (DMFC) has been developed to investigate mass transfer phenomena. In particular the MeOH crossover phenomenon is investigated and model validations are done using the current distribution measurements [12]. The model is implemented using the commercial Comsol Multiphysics 3.3 program (Comsol AB).

In this model, the *Navier–Stokes equation* (Eq. (1)) is used for modelling Newtonian flow of MeOH and water in the anode flow field and also free convection of air in the cathode flow field. The *Stefan–Maxwell equation* (Eq. (8)) is used for modelling multicomponent diffusion of gaseous species in the porous cathode transport layer (PTL) and *Brinkman's equation* (Eq. (2)) for modelling the flow of MeOH and water in the anode PTL. The *Tafel equation* (Eq. (17)) is used to describe electrochemical reactions at the cathode and the linearized *Butler–Volmer equation* (Eq. (18)) at the anode. The MeOH flow in the membrane (MeOH crossover) is described with *Fick's law of diffusion* and drag of protonic current (Eq. (19)). The only fitted parameter in the model is the parameter ψ for the MeOH oxidation rate at the cathode. ψ is fitted according to the measured current distributions.

The model geometry is illustrated in Fig. 1 and the main flow directions of MeOH–water solution and free air convection are also marked in the figure. The air channels of the cell (y-axis) are vertically oriented. Producing the DMFC model in 3D causes some restrictions and compromises to the modelling work, because the model solution should be found in a reasonable time with the available computer resources. Much more detailed models can be done in 1D [40,45], 2D [41,43] or if only some part of the DMFC, e.g. the anode is modelled [50,51]. In our case, the available computer resources practically means that the number of elements and degrees of freedom in the model should not exceed 10^6. The main simplifications to the real DMFC geometry, which is described in detail in [12], are that the electrodes are considered only as boundary conditions and the whole area of the PTL (z-plane) is considered as a current collector instead of the segmented electrode used in the experimental work. Also, the flows of reactants (both the inflows and outflows) are set to be only in the main flow directions (see arrows in Fig. 1) instead of in the separate air channels of the cathode and the serpentine parallel MeOH channels in the anode of the experimental DMFC. The geometry can also be scaled down (1:10) in the x-direction by adjusting the corresponding flow parameters, which leads to a significant decrease in computing time without affecting the modelling results. The following assumptions are used in the model:

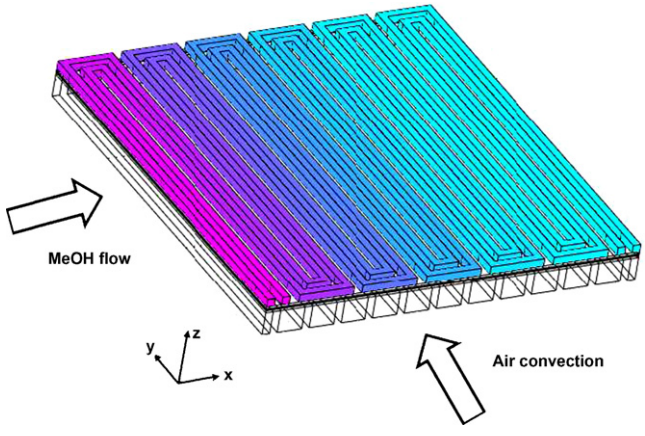

Fig. 1. The modelled geometry and the main flow directions of reactants.

1. Steady-state isothermal and single-phase conditions.
2. No phase transitions (gas condensation or liquid vapourization) between liquid water (anode side and membrane) and water vapour (cathode side).
3. Ideal gas assumption for gaseous species and all flows are assumed to be laminar.
4. Liquid species (MeOH and water) are considered to be Newtonian fluids.
5. Complete MeOH oxidation (no partial oxidation or side reactions).
6. No gas fluxes through the membrane.
7. CO_2 and H_2 fluxes are neglected.
8. All electrochemical reactions take place at indefinitely thin electrodes and no reactions occur in the membrane, porous transport layers or flow field regions.

2.2. Governing equations

2.2.1. MeOH flow field and porous anode transport layer

The flow of MeOH and water at the anode flow field can be described with the Navier–Stokes equation:

$$\rho\mathbf{u}\cdot\nabla\mathbf{u} = \mu\nabla^2\mathbf{u} - \nabla p - \rho\frac{\partial\mathbf{u}}{\partial t} \tag{1}$$

where μ is the dynamic viscosity of the MeOH–water solution. The flow through the porous anode transport layer (PTL) can be described according to Brinkman's equation (Brinkman's extension of Darcy's law):

$$\mu\nabla^2\mathbf{u} - \frac{\mu}{\kappa}\mathbf{u} = \nabla p \tag{2}$$

where κ is the intrinsic permeability of the porous medium. At the anode flow field and the PTL, the molar fluxes of MeOH and water are continuous ($\nabla\cdot\mathbf{N}_i = 0$) and are modelled with the equation for convective diffusion:

$$\mathbf{N}_i = -D_i\nabla c_i + c_i\mathbf{u} \tag{3}$$

2.2.2. Air flow field and porous cathode transport layer

The developed three-dimensional model for the air flow field and the cathode PTL is based on a 2D model developed by Mennola et al. [52]. The steady-state continuity equation for mass ($\nabla\cdot\rho\mathbf{u} = 0$) is used and the free convection of air at the cathode channels is described with the Navier–Stokes equation (Eq. (1)). The buoyancy in the vertical cathode channels (y-direction) is caused by density differences of air resulting from thermal expansion ($T_{\text{cell}} > T_{\text{amb}}$) and changes in gas composition (electrochemical reactions). The pressure variations in the flow field region are assumed to be small, i.e. Eq. (1) simplifies to the form:

$$\mu\nabla^2\mathbf{u} + \mathbf{g}(\rho - \rho_0) = 0 \tag{4}$$

where the density of air ρ is calculated according to Eq. (5):

$$\rho = c\sum_i X_i M_i \tag{5}$$

The total concentration c can be calculated from the ideal gas law:

$$c = \frac{p}{RT} \tag{6}$$

The molar fluxes of chemical species are continuous ($\nabla \cdot \mathbf{N}_i = 0$) in the air flow field and are defined according to Eq. (3). The mole fraction of nitrogen is calculated from the mole fractions of oxygen and water vapour:

$$X_{N_2} = 1 - X_{O_2} - X_{H_2O} \tag{7}$$

In the porous cathode transport layer (PTL) the Stefan–Maxwell equation is used for modelling multi-component diffusion:

$$\nabla X_i = \sum_j \frac{1}{cD_{ij}}(X_i\mathbf{N}_j - X_j\mathbf{N}_i) \tag{8}$$

where D_{ij} is the binary diffusion coefficient of the gas pair $i - j$. Nitrogen is inert and its flux is set to zero. The molar fluxes for oxygen and water vapour can be solved according to Eq. (8):

$$\mathbf{N}_{O_2} = -c\frac{D_{O_2,H_2O}D_{N_2,O_2}}{D_{N_2,O_2}X_{H_2O} + D_{N_2,H_2O}X_{O_2} + D_{O_2,H_2O}X_{N_2}} \times \times \left(\frac{X_{O_2}D_{N_2,H_2O}}{X_{N_2}D_{O_2,H_2O}}(\nabla X_{H_2O} + \nabla X_{O_2}) + \nabla X_{O_2}\right) \tag{9}$$

$$\mathbf{N}_{H_2O} = -c\frac{D_{O_2,H_2O}D_{N_2,H_2O}}{D_{N_2,O_2}X_{H_2O} + D_{N_2,H_2O}X_{O_2} + D_{O_2,H_2O}X_{N_2}} \times \times \left(\frac{X_{H_2O}D_{N_2,H_2O}}{X_{N_2}D_{O_2,H_2O}}(\nabla X_{H_2O} + \nabla X_{O_2}) + \nabla X_{H_2O}\right) \tag{10}$$

2.2.3. Electrode reactions

According to our experimental results [12] and observations of, e.g. Ye et al. [34] and Kulikovsky et al. [35], two different regions depending on local conditions inside DMFC can be distinguished:

1. Normal DMFC operation (Galvanic cell):

anode: $CH_3OH + H_2O \rightarrow CO_2 + 6H^+ + 6e^-$ (11)

cathode: $\frac{3}{2}O_2 + 6H^+ + 6e^- \rightarrow 3H_2O$ (12)

2. Electrolytic cell:

anode : $6H^+ + 6e^- \rightarrow 3H_2$ (13)

cathode : $CH_3OH + H_2O \rightarrow CO_2 + 6H^+ + 6e^-$ (14)

Reaction (12) is the main reaction at the cathode of the DMFC, but because of the MeOH crossover phenomenon, MeOH oxidation will also occur at the cathode and the corresponding anode reaction is then hydrogen formation. When the MeOH crossover rate through the membrane is low, reaction (12) is dominating at the cathode. In this model, the cathode and anode electrodes are taken into account as boundary conditions and electrochemical reactions take place at indefinitely thin electrodes. The drain and source terms of MeOH and water are included in the model according to the anode and cathode reactions, but the fluxes of CO_2 and H_2 are neglected. In the DMFC, the cathode and anode PTLs act also as current collectors for electricity and only an electronic potential exists:

$$\nabla \cdot (-\sigma^{s}_{ptl}\nabla\phi_s) = 0 \tag{15}$$

The transfer of electronic current into protonic current takes place at the boundaries between the anode and cathode PTLs and the membrane. The current production at the cathode (reaction (12)) is approximated with the Tafel equation:

$$i^{c}_{ele} = i^{c}_{0}\exp\left(-\frac{\alpha_c F}{RT}\eta_c\right) \tag{16}$$

where the cathodic overpotential $\eta_c = \phi_s - \phi_m - E^0$. Because the MeOH crossover phenomenon decreases the total current production at the cathode, the following modifications to Eq. (16) are introduced:

$$i^{c}_{ele} = i^{c}_{0}\left(\frac{c_{O_2}}{c^{ref}_{O_2}}\right)\exp\left(-\frac{\alpha_c F}{RT}\eta_c\right) - 6Fc^{mem}_{MeOH}\psi \tag{17}$$

where the parameter ψ describes the MeOH oxidation rate at the cathode. This parameter is to be fitted according to the measured current distributions. The effect of local oxygen concentration is also taken into account in Eq. (17) and the dependency between MeOH oxidation rate and MeOH concentration is assumed to be linear. When the DMFC is operating in galvanic mode, without any MeOH crossover, the Tafel equation (Eq. (16)) is the most reasonable way to describe current production at the anode. The drawback of the exponential Tafel equation is that it cannot be used alone without any additional terms or fitting parameters, in order to describe also the local electrolytic domains found experimentally [12]. Thus, a major simplification for the anodic current production is made by assuming only low anodic overpotentials and approximating the anodic current production (reaction (11)) with the linearized Butler–Volmer equation:

$$i^{a}_{ele} = i^{a}_{0}\left(\frac{c_{MeOH}}{c^{ref}_{MeOH}}\right)\frac{\alpha_a F}{RT}\eta_a \tag{18}$$

where the anodic overpotential $\eta_a = \phi_m - \phi_s$. The effect of local MeOH concentration is also taken into account in Eq. (18).

2.2.4. Membrane

No reactions occur in the membrane and only a protonic phase exists ($\nabla \cdot (-\sigma^{m}_{mem}\nabla\phi_m) = 0$). The MeOH crossover through the membrane occurs because of electro-osmosis and the gradients of pressure and concentration:

$$\mathbf{N}^{mem}_{MeOH} = \frac{\lambda_{MeOH}}{F}i + \frac{\kappa}{\mu}c_{MeOH}\nabla p - D^{mem}_{MeOH}\nabla c \tag{19}$$

where λ_{MeOH} is the electro-osmotic drag coefficient (number of MeOH molecules dragged by each proton). The flux induced by the pressure gradient is assumed to be small compared to other

fluxes and so it is neglected in the model. The last term in Eq. (19) is the diffusion flux according to Fick's law of diffusion. Because of relatively high water content on both sides of the membrane (liquid water at the anode and water vapour and water production at the cathode), the membrane is assumed fully hydrated and water flow in the membrane is modelled only with the drag of protonic current:

$$\mathbf{N}_{H_2O}^{mem} = \frac{\lambda_{H_2O}}{F} i \quad (20)$$

2.3. Boundary conditions

2.3.1. MeOH and water

The concentrations and velocities of MeOH and water are fixed at the beginning of the anode flow channel. Whereas at the end of the anode flow channel, the concentration gradients are set to zero and the pressure is fixed to the constant pressure of ambient air. The boundary conditions between the anode PTL and the membrane are set according to MeOH and water consumption (Eqs. (11) and (18)) and the boundary conditions between the membrane and the cathode PTL according to Eqs. (14) and (17) (oxidation of permeated MeOH).

2.3.2. Oxygen and water vapour

The input concentrations in ambient air are calculated according to Eq. (6) and the vertical velocity gradients are assumed to be zero (fully developed flow) at the end of the air channel. The boundary conditions between the cathode PTL and the membrane are set according to oxygen consumption and water vapour production (Eqs. (12) and (17)). Gas fluxes to the membrane are set to zero and phase transitions between liquid water and water vapour are not taken into account. The pressure is set to be constant at both ends of the air channels, because they are open to the ambient air.

2.3.3. Electronic and protonic potentials

The electrodes are described as boundary conditions in the model. The electronic potentials are fixed at the boundaries between the flow fields and the PTLs. Because the whole area of the anode and cathode PTL acts as a current collector for electricity in the model, the electronic potential is set to zero at the boundary between the MeOH flow field and the anode PTL and to the cell voltage at the boundary between the cathode PTL and the air flow field. The protonic potential exists only in the membrane and the fluxes of electrons and protons are fixed between the membrane and the PTLs according to their consumption and production (Eqs. (17) and (18)).

2.4. Parameters and variables

All parameters in the model are assumed to be independent of concentrations of reacting species, e.g. the temperature dependent dynamic viscosity value for the MeOH–water mixture is calculated as an average value of the MeOH concentrations (0.5–10 M) used. All common parameters and variables are presented in Table 1. The model variables are given the same values as they had in the experimental measurements [12]. The density of air and partial pressure values of oxygen, nitrogen and water vapour are calculated assuming 50% relative humidity of the ambient air. The thickness of the compressed porous transport layer is assumed to be 300 μm and the thickness of the compressed and fully hydrated Nafion® 117 membrane 200 μm.

Table 1
Parameters and variables

Parameter	Value
T_{cell} (°C)	30, 50, 70
c_{MeOH} (mol dm^{-3})	0.5, 1, 3, 5, 10
$\dot{V}_{MeOH,H_2O}$ (m^3 s^{-1})	3.3×10^{-9}, 17×10^{-9}, 130×10^{-9}
l_{ptl} (m)	300×10^{-6}
l_{mem} (m)	200×10^{-6}
M_{H_2O} (kg mol^{-1})	18×10^{-3}
M_{MeOH} (kg mol^{-1})	32×10^{-3}
M_{N_2} (kg mol^{-1})	28×10^{-3}
M_{O_2} (kg mol^{-1})	32×10^{-3}
E_0 (V)	0.6
T_{amb} (°C)	25
RH	50%
p_0 (Pa)	1.01×10^5
ρ_0^{air} (kg m^{-3})	1.177
$p_{O_2}^{air}$ (Pa)	20945
$p_{N_2}^{air}$ (Pa)	78794
$p_{H_2O}^{air}$ (Pa)	1585
$c_{O_2}^{ref}$ (mol m^{-3})	0.136
c_{MeOH}^{ref} (mol m^{-3})	100
σ_{ptl}^{s} (S m^{-1})	10^3
κ_{ptl} (m^2)	1×10^{-11}
$\lambda_{MeOH} = \lambda_{H_2O}$	2.5
ϵ_{mem}	0.28
ϵ_{ptl}	0.6
α_a	0.24
α_c	0.875
i_0^c (A m^{-2})	1
i_0^a (A m^{-2})	10^3
p_{cr,N_2} (Pa)	3.393×10^6
p_{cr,O_2} (Pa)	5.04×10^6
p_{cr,H_2O} (Pa)	22.1×10^6
T_{cr,N_2} (K)	126.2
T_{cr,O_2} (K)	154.6
T_{cr,H_2O} (K)	647.1

The values for the exchange current densities i_0^c and i_0^a and the open circuit voltage E_0 are assumed to be independent of the cell temperature. The same assumption is also made for the following parameters: the conductivity of the porous transport layer σ_{ptl}^s is assumed according to Refs. [47,53,54]. The intrinsic permeability κ_{ptl} and the transfer coefficients of the electrochemical reactions α_a and α_c are assumed to be the same as in Ref. [43], water drag coefficients λ_{MeOH} and λ_{H_2O} as they are in Ref. [26] and membrane porosity ϵ_{mem} as in Ref. [48]. The value of the porosity of the transport layer ϵ_{ptl} is as the one used in, e.g. Refs. [45,48,52,53]. Values of the critical pressure and temperature (p_{cr} and T_{cr}) are taken from Ref. [55].

All temperature dependent parameters are presented in Table 2. The conductivity of the membrane is calculated according to Ref. [56], the diffusion coefficient of MeOH in water according to Ref. [57] and diffusion coefficient of MeOH in the membrane according to Ref. [48]. Before inserting D_{MeOH}^{mem}

Table 2
Temperature dependent parameters

Parameter	$T_{cell} = 30\,^{\circ}C$	$T_{cell} = 50\,^{\circ}C$	$T_{cell} = 70\,^{\circ}C$
μ_{air} (Pa s^{-1})	1.86×10^{-5}	1.95×10^{-5}	2.03×10^{-5}
μ_{MeOH} (Pa s^{-1})	7.7×10^{-4}	5.3×10^{-4}	4.2×10^{-4}
σ_{mem} (S m^{-1})	7.8	10.2	12.8
$D^{air}_{O_2}$ (m^2 s^{-1})	2.05×10^{-5}	2.30×10^{-5}	2.55×10^{-5}
$D^{air}_{H_2O}$ (m^2 s^{-1})	2.58×10^{-5}	2.88×10^{-5}	3.20×10^{-5}
$D^{H_2O}_{MeOH}$ (m^2 s^{-1})	1.9×10^{-9}	3.1×10^{-9}	4.7×10^{-9}
D^{mem}_{MeOH} (m^2 s^{-1})	6.3×10^{-10}	1.0×10^{-9}	1.7×10^{-9}
D_{O_2,N_2} (m^2 s^{-1})	2.12×10^{-5}	2.38×10^{-5}	2.66×10^{-5}
D_{O_2,H_2O} (m^2 s^{-1})	2.60×10^{-5}	3.02×10^{-5}	3.47×10^{-5}
D_{N_2,H_2O} (m^2 s^{-1})	2.72×10^{-5}	3.16×10^{-5}	3.63×10^{-5}

values into Eq. (19), the effective diffusion coefficients are calculated using the Bruggeman correlation (Eq. (21)) to take into account the porosity of the membrane:

$$D_{eff} = (\epsilon^{1.5})D \tag{21}$$

The diffusion coefficients of oxygen and water vapour in air are calculated according to Eq. (22), which is based on the work of Fuller et al. [58]:

$$D_{ij} = 0.0101 \frac{T^{1.75}((1/M_i) + (1/M_j))^{1/2}}{p[(\Sigma v_i)^{1/3} + (\Sigma v_j)^{1/3}]^2} \tag{22}$$

where the value of the diffusion volume Σv is 16.3 for oxygen, 19.7 for air and 13.1 for water vapour. The binary diffusion coefficients in the cathode PTL are calculated according the Slattery-Bird correlation [55]:

$$D_{ij} = \frac{a(T/\sqrt{T_{cr,i}T_{cr,j}})^b (p_{cr,i}p_{cr,j})^{1/3}(T_{cr,i}T_{cr,j})^{5/12}((1/M_i) + (1/M_j))^{1/2}}{p} \tag{23}$$

where $T_{cr,i}$ and $T_{cr,j}$ are the critical temperatures (K), $p_{cr,i}$ and $p_{cr,j}$ the critical pressures (atm) and M_i and M_j molar masses (g mol^{-1}) of the species i and j, respectively. The values of the empirical constants a and b depend on gas pair and for non-polar gas pairs $a = 2.745 \times 10^{-4}$ and $b = 1.823$, whereas for a binary diffusion of water vapour with non-polar gas $a = 3.640 \times 10^{-4}$ and $b = 2.334$. Before inserting binary diffusion coefficients into Eqs. (9) and (10), the effective diffusion coefficients are calculated using the Bruggeman correlation (Eq. (21)).

3. Results and discussion

3.1. Experimental validation

The current distribution measurement system for a free-breathing DMFC is described in detail in [12]. The cathode flow field plate is divided into 48 segments and the current distribution is measured with a resistor network. A similar approach has been used in PEFC studies by Noponen et al. [5,6]. Most of the measurement data used in this modelling work is presented

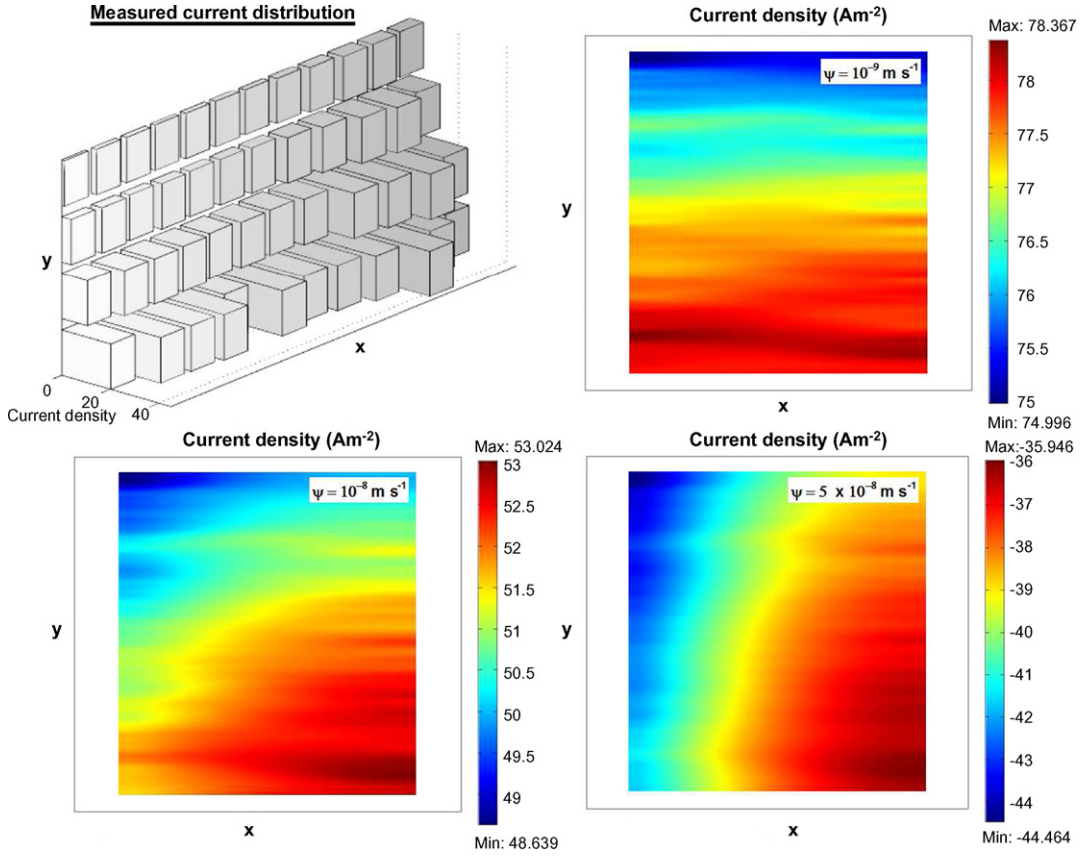

Fig. 2. The measured and three modelled current density distributions with different ψ values at 70 $^{\circ}$ C (5 M MeOH, flow rate 17×10^{-9} m^3 s^{-1}).

in [12] and measured using the commercial Nafion®117 membrane and hot-pressed gas diffusion electrodes for the DMFC (E-TEK).

The current distribution measurements are done using 0.5, 1, 3, 5 and 10 M MeOH solutions and the MeOH flow rates are also varied in a wide range from 3.3×10^{-9} to 130×10^{-9} $m^3\,s^{-1}$ (0.2–8 ml min^{-1}). Thus, the MeOH feed stoichiometry is varied from 3 to 2500. Because the temperature used and the cell current affects the mass transport and electrode kinetics, the measurements are done at three different cell temperatures (30, 50 and 70 °C) and using different average current densities.

The parameter ψ in the model (Eq. (17)) describes the MeOH oxidation rate at the cathode and it is fitted according to the measured current distributions. Typical values for ψ are relatively small, in most of the cases $\psi = 10^{-9}$ to 10^{-8} $m\,s^{-1}$. If too high a value for ψ is used, the shape of the current distribution turns impractical and the current production of the cell decreases drastically. An example of this situation is presented in Fig. 2, where both one measured and three modelled current density distributions at 70 ° C are presented. The flow rate of 5 M MeOH is 17×10^{-9} $m^3\,s^{-1}$ and the ψ values used are 10^{-9}, 10^{-8} and 5×10^{-8} $m\,s^{-1}$. When the value of ψ is 10^{-9} $m\,s^{-1}$, the shape of the modelled current distribution is quite similar to the measured one: there are no significant variations in the x-direction and the current density decreases in the y-direction. It can also be seen that the measured current density decreases much faster in the y-direction than the modelled one with $\psi = 10^{-9}$ $m\,s^{-1}$ and with increasing ψ values, the current density distribution turns to negative values over the whole electrode.

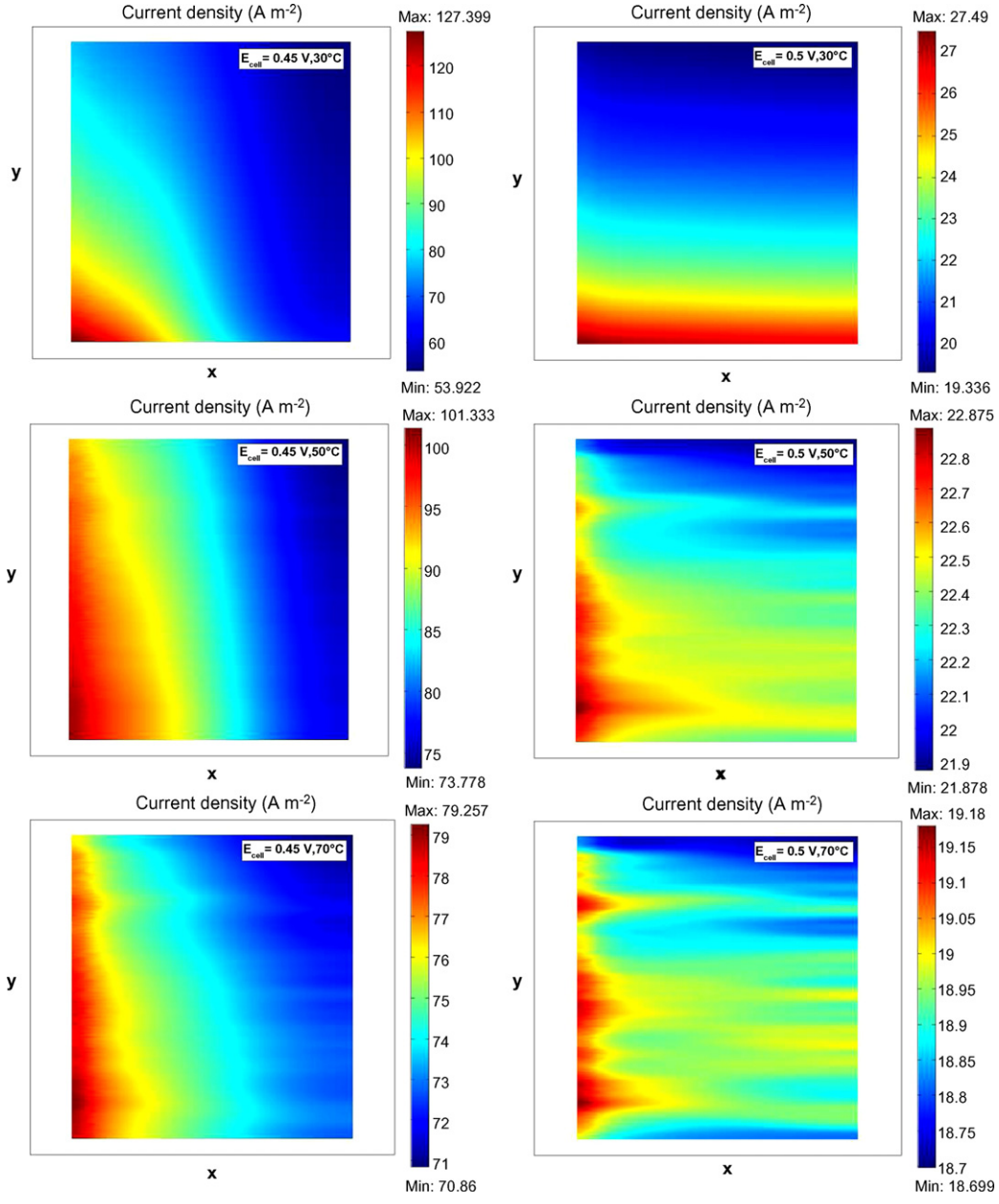

Fig. 3. The modelled current density distributions at 30, 50 and 70 °C. E_{cell} is 0.45 V (left) and 0.5 V (right). The flow rate of 0.5 M MeOH is 17×10^{-9} $m^3\,s^{-1}$.

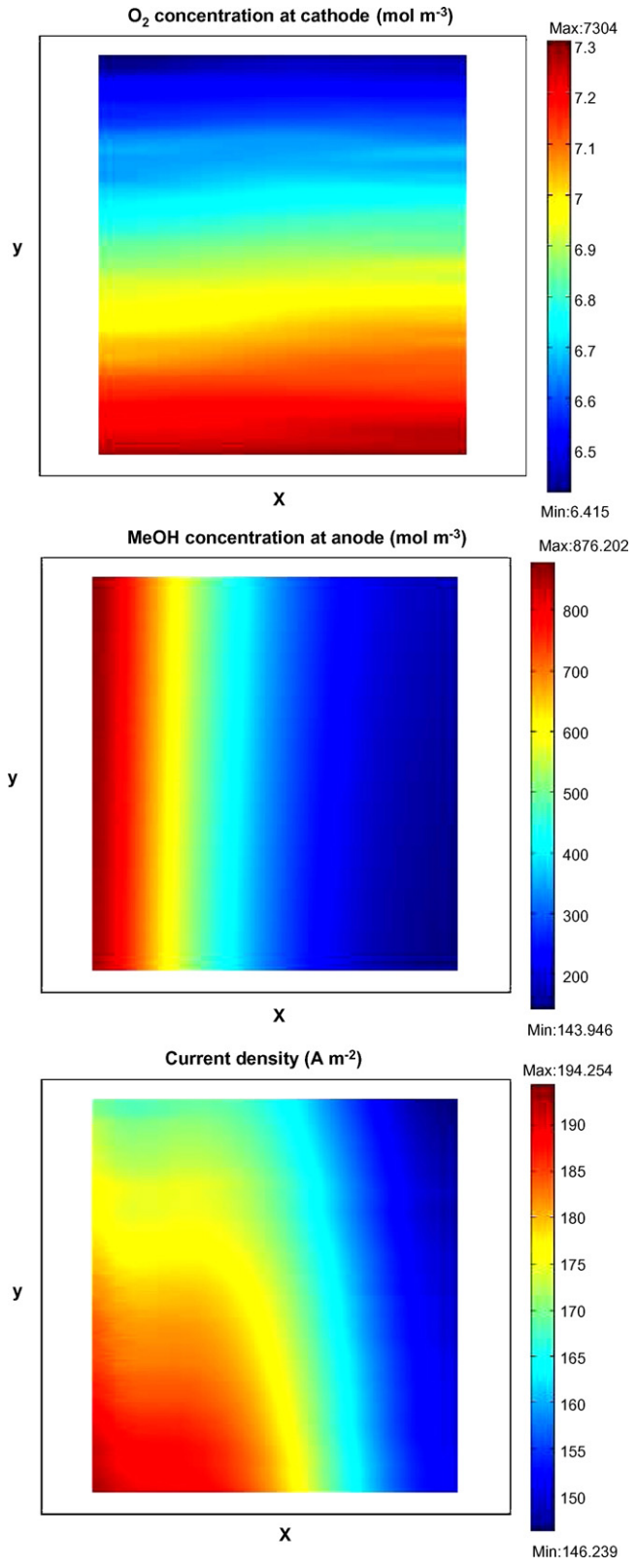

Fig. 4. The modelled oxygen concentration at the cathode (above), MeOH concentration at the anode (center) and current density distribution (below) at 70 °C (1 M MeOH, flow rate 17×10^{-9} m^3 s^{-1}, $E_{cell} = 0.4$ V).

3.2. Concentration profiles of the reactants

During the modelling work, the following general observations were done concerning the concentration profiles of the reactants.

3.2.1. Cathode side

The vertical buoyancy of air is caused by density differences resulting from thermal expansion ($T_{cell} > T_{amb}$) and increases as a function of cell temperature. The highest velocity of air is naturally located in the center of the air flow field in the x-direction. There are also concentration gradients of oxygen and water vapour towards and away from the cathode according to reaction (12). As a result, changes in gas composition can be seen: the oxygen concentration decreases and the water vapour concentration increases as a function of cell current.

3.2.2. Anode side

The concentrations of MeOH and liquid water decrease as a function of cell current according to reaction (11) and there is a MeOH concentration profile along the anode flow channel. The shape of this profile depends on the MeOH input concentration and flow rate. Because of diffusion and electro-osmotic drag of protons, there are also concentration gradients of MeOH and water through the membrane and MeOH is oxidized at the cathode according to reaction (14). If the DMFC is operated with a relatively high constant current and with a low MeOH concentration and flow rate, most of the MeOH is consumed at the anode. As a consequence, there is only a small amount of MeOH, which can permeate through the membrane and react at the cathode. On the contrary, if the DMFC is operated with a low cell current and with a high MeOH concentration, the MeOH crossover rate is high.

3.3. The effect of cell temperature

The performance values of the DMFC depend quite much on the cell temperature and power densities increase as a function of temperature, mainly as a result of the increased catalytic activity (decreased activation overpotential). On the other hand, some part of this gain is lost as the MeOH crossover also increases as a function of temperature [27,29].

When concentration profiles of reacting species at both electrodes are compared to the corresponding current distribution, it is observed that the oxygen mass transfer limitations decrease the cell performance most in the free-breathing DMFC, when the cell temperature is 30 °C. The buoyancy of air increases, when the temperature is increased and this can be seen in the concentration profiles of oxygen at the cathode and in the current density distributions. An example is shown in Fig. 3, where six modelled current density distributions at three different cell temperatures (30, 50 and 70 °C) are presented.

It can be seen from Fig. 3 that mass transfer of air is limiting the cell performance mainly at low temperatures and when the cell voltage is near the OCV. Most of the current is produced at the beginning of the air flow field and the current density decreases in the air flow direction (y-axis), when the cell

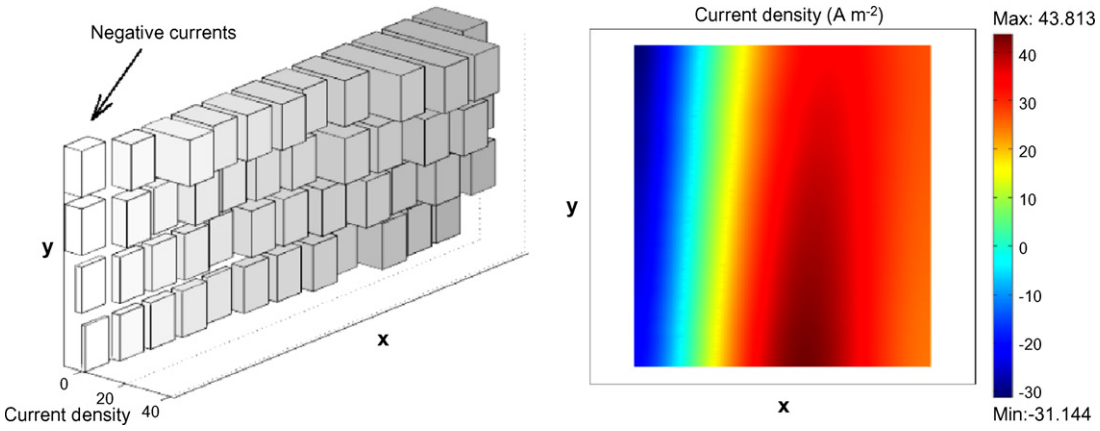

Fig. 5. The measured (left) and modelled (right) current density distribution at 70 ° C (3 M MeOH, flow rate 3.3×10^{-9} m^3 s^{-1}, $E_{cell} = 0.5$ V).

temperature is 30 °C. At higher temperatures, most of the current is produced near the MeOH inlet and the shape of the current density distribution turns gradually from the air flow direction (y-axis) towards the MeOH flow direction (x-axis) as a function of temperature. At the same time, there can be seen a drastic decrease in the local variations of the current density at the electrode.

3.4. The effects of MeOH and oxygen concentration

High mass transfer overpotentials can exist in a free-breathing DMFC, even at relatively low current densities. This results mainly from an inadequate air flow towards the cathode. During the previous experimental work [12] and this modelling work, it has been observed that the local oxygen and MeOH concentrations have a significant effect on the current density distribution in the DMFC. The MeOH mass transfer is also limiting the cell performance especially at high current densities, but oxygen mass transfer limitations are highly dominating especially in the case of the free-breathing DMFC. Similar observations have been done, e.g. by Geiger et al. [16], who have made segmented DMFC measurements and concluded that the current distribution is highly dependent on the O_2 concentration.

The MeOH crossover decreases the performance of the DMFC, especially when using high MeOH concentrations (5–10 M), a low MeOH flow rate (3.3×10^{-9} m^3 s^{-1}) and if the cell is operated at low current densities. When the shapes of MeOH and oxygen concentration profiles are compared to the corresponding cell current distribution, the limiting mass transfer process can be indentified. In many cases, it can be seen whether the oxygen or MeOH mass transport is the more limiting one, but sometimes both of them substantially affect the shape of the current distribution. An example of this situation is presented in Fig. 4, where modelling results for the oxygen concentration at the cathode, the MeOH concentration at the anode and the corresponding current density distribution at 70 ° C are shown. The flow rate of 1 M MeOH is 17×10^{-9} m^3 s^{-1}and $E_{cell} = 0.4$ V. The mass transfer limitations of MeOH and oxygen can be seen in different directions: the oxygen concentration decreases and limits the cell performance in the y-direction and MeOH concentration in the x-direction.

During the experimental measurements, it has been observed that the current densities can vary significantly inside the DMFC and in some cases even negative currents have been measured [12]. An example of measured local negative currents is presented at the left in Fig. 5. The cell voltage is 0.5 V and the flow rate of 3 M MeOH is 3.3×10^{-9} m^3 s^{-1}. The current densities are negative near the MeOH inlet, because the DMFC is operated with relatively low current density and the MeOH crossover is dominating at those cathode segments. The corresponding modelled current density distribution ($\psi = 1.15 \times 10^{-9}$ m s^{-1}) is presented at the right in Fig. 5 and it is quite similar to the measured one. The model predicts that the current production of the DMFC can be locally negative, when the MeOH crossover rate is high near the MeOH inlet. The current densities increase along the MeOH flow direction (x-axis), which can be explained with a decrease of the MeOH concentration at the anode. The MeOH concentration decreases due to the electrochemical reactions and as a result, the effect of MeOH crossover is reduced and the current production again turns positive.

3.5. Model agreement with polarization curves

After model validations according to the measured current distributions, the polarization curves can be obtained by changing the cell voltage and calculating the corresponding current in the z-direction. An example of calculated and measured polarization curves and power densities at 70 ° C is presented in Fig. 6. The galvanostatic measurement is made using current steps of 1 mA cm^{-2} and the flow rate of 1 M MeOH solution is 17×10^{-9} m^3 s^{-1}.

It can be seen from Fig. 6 that ohmic losses are lower in the model calculation compared to the real DMFC system. This is quite reasonable, because the whole area of the PTL is used as a current collector in the model and the contact resistances between the current collector and the PTL are neglected. When comparing the measured and calculated polarization curves at high current densities, it can be seen that the current production

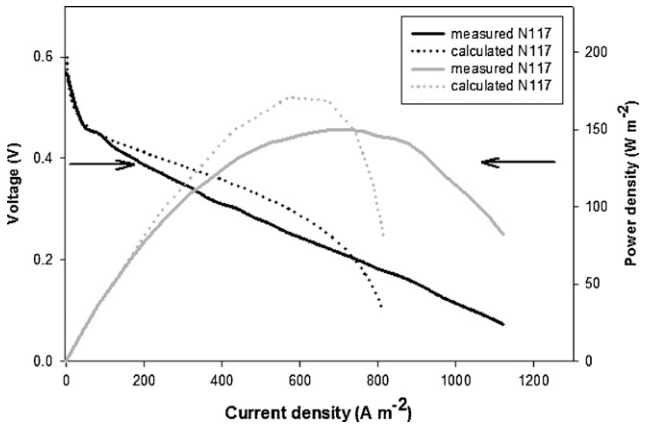

Fig. 6. Measured and calculated polarization curves and power densities at 70 °C (1 M MeOH, flow rate 17×10^{-9} m^3 s^{-1}.

predicted by the model decreases faster than the measured one, evidently due to overestimation of the mass transfer overpotentials by the model. Also other simplifications of the model probably cause that there is not a perfect fit between the measured and calculated polarization curves, even though the model predicts power densities with reasonable accuracy. For future work and to achieve an even better fit, it is recommended that the model validations are done both with the polarization curves and the current distribution measurements.

4. Conclusions

A three-dimensional model is developed for a free-breathing direct methanol fuel cell. The MeOH crossover and other mass transfer phenomena are investigated computationally and the model validations are done using the current distribution measurements. Even if the model presented contains several simplifying assumptions, it describes mass transfer phenomena and current production in a free-breathing DMFC, when different operating parameters such as cell temperature, MeOH concentration and reactant flow rates are varied on a large scale. The model also describes with reasonable accuracy the existence of the measured electrolytic domains, i.e. regions of negative current densities.

The current distribution is observed to be closely connected to the local concentrations and mass flows of the reacting species. The local power production is observed to be proportional to the local oxygen concentration at the cathode side. As a consequence, inadequate air convection together with the MeOH crossover phenomenon decreases the cell performance. At high MeOH concentrations, the MeOH crossover and the mass transfer of air are mainly limiting the cell performance, especially at low and high current densities, respectively. Altogether, the developed model is in reasonable agreement with both the measured current distributions and polarization curves. The spatial information gained of mass transfer phenomena inside the DMFC is valuable for the optimization of the DMFC operating parameters.

Acknowledgements

Financial support for this work from the Magnus Ehrnrooth Foundation and the Academy of Finland (Decision 206132) is gratefully acknowledged.

References

[1] S. Kamarudin, W. Daud, S. Ho, U. Hasran, J. Power Sources 163 (2007) 743–754.
[2] S.J.C. Cleghorn, C.R. Derouin, M.S. Wilson, S. Gottesfeld, J. Appl. Electrochem. 28 (1998) 663–672.
[3] J. Stumper, S.A. Campbell, D.P. Wilkinson, M.C. Johnson, M. Davis, Electrochim. Acta 43 (1998) 3773–3783.
[4] C. Wieser, A. Helmbold, E. Gülzow, J. Appl. Electrochem. 30 (2000) 803–807.
[5] M. Noponen, T. Mennola, M. Mikkola, T. Hottinen, P. Lund, J. Power Sources 106 (2002) 304–312.
[6] M. Noponen, T. Hottinen, T. Mennola, M. Mikkola, P. Lund, J. Appl. Electrochem. 32 (2002) 1081–1089.
[7] T. Hottinen, M. Noponen, T. Mennola, O. Himanen, M. Mikkola, P. Lund, J. Appl. Electrochem. 33 (2003) 265–271.
[8] M. Noponen, J. Ihonen, A. Lundblad, G. Lindbergh, J. Appl. Electrochem. 34 (2004) 255–262.
[9] Z. Liu, Z. Mao, B. Wu, L. Wang, V. Schmidt, J. Power Sources 141 (2005) 205–210.
[10] X.-G. Yang, N. Burke, C.-Y. Wang, K. Tajiri, K. Shinohara, J. Electrochem. Soc. 4 (2005) A759–A766.
[11] R. Eckl, R. Grinzinger, W. Lehnert, J. Power Sources 154 (2006) 171–179.
[12] V. Saarinen, O. Himanen, T. Kallio, G. Sundholm, K. Kontturi, J. Power Sources 163 (2007) 768–776.
[13] E. Gülzow, T. Kaz, R. Reissner, H. Sander, L. Schilling, M.v. Bradke, J. Power Sources 105 (2002) 261–266.
[14] R. Liu, E.S. Smotkin, J. Electroanal. Chem. 535 (2002) 49–55.
[15] M. Mench, Q. Dong, C. Wang, J. Power Sources 124 (2003) 90–98.
[16] A.B. Geiger, R. Eckl, A. Wokaun, G.G. Scherer, J. Electrochem. Soc. 151 (2004) A394–A398.
[17] A. Heinzel, V. Barrágan, J. Power Sources 84 (1999) 70–74.
[18] H. Dohle, J. Divisek, R. Jung, J. Power Sources 86 (1999) 469–477.
[19] H. Dohle, J. Divisek, J. Mergel, H. Oetjen, C. Zingler, D. Stolten, J. Power Sources 105 (2002) 274–282.
[20] B. Gurau, E.S. Smotkin, J. Power Sources 112 (2002) 339–352.
[21] J.P.G. Villaluenga, B. Seoane, V.M. Barrágan, C. Ruiz-Bauzá, J. Colloid Interface Sci. 268 (2003) 476–481.
[22] S. Sandhu, R. Crowther, J. Fellner, Electrochim. Acta 50 (2005) 3985–3991.
[23] T. Schaffer, T. Tschinder, V. Hacker, J.O. Besenhard, J. Power Sources 153 (2006) 210–216.
[24] J.P.G. Villaluenga, B. Seoane, V.M. Barrágan, C. Ruiz-Bauzá, J. Membr. Sci. 274 (2006) 116–122.
[25] V. Silva, A. Mendes, L. Madeira, S. Nunes, J. Membr. Sci. 276 (2006) 126–134.
[26] X. Ren, T. Springler, T.A. Zawodzinski, S. Gottesfeld, J. Electrochem. Soc. 147 (2000) 466–474.
[27] T. Kallio, K. Kisko, K. Kontturi, R. Serimaa, F. Sundholm, G. Sundholm, Fuel Cells 4 (2004) 328–336.
[28] V. Saarinen, T. Kallio, M. Paronen, P. Tikkanen, E. Rauhala, K. Kontturi, Electrochim. Acta 50 (2005) 3453–3460.
[29] V. Saarinen, M. Karesoja, T. Kallio, M. Paronen, K. Kontturi, J. Membr. Sci. 280 (2006) 20–28.
[30] M. McGovern, P. Waszczuk, A. Wieckowski, Electrochim. Acta 51 (2006) 1194–1198.
[31] R.J. Behm, Z. Jusys, J. Power Sources 154 (2006) 327–342.
[32] J.-T. Wang, S. Wasmus, R. Savinell, J. Electrochem. Soc. 143 (1996) 1233–1239.
[33] Q. Ye, T. Zhao, J. Electrochem. Soc. 152 (2005) A2238–A2245.

[34] Q. Ye, T. Zhao, H. Yang, J. Prabhuram, Electrochem. Solid-State Lett. 8 (2005) A52–A54.
[35] A. Kulikovsky, H. Schmitz, K. Wippermann, J. Mergel, B. Fricke, T. Sanders, D. Sauer, Electrochem. Commun. 8 (2006) 754–760.
[36] C.-Y. Wang, Chem. Rev. 104 (2004) 4727–4766.
[37] A.Z. Weber, J. Newman, Chem. Rev. 104 (2004) 4679–4726.
[38] K.Z. Yao, K. Karan, K.B. McAuley, P. Oosthuizen, B. Peppley, T. Xie, Fuel Cells 4 (2004) 3–29.
[39] A.A. Kulikovsky, Electrochem. Commun. 4 (2002) 939–946.
[40] C.-H. Chen, T.-K. Yeh, J. Power Sources 160 (2006) 1131–1141.
[41] J. Rice, A. Faghri, Int. J. Heat Mass Transfer 49 (2006) 4804–4820.
[42] S. Zhou, T. Schultz, M. Peglow, K. Sundmacher, Phys. Chem. Chem. Phys. 3 (2001) 347–355.
[43] Z.H. Wang, C.Y. Wang, J. Electrochem. Soc. 150 (2003) A508–A519.
[44] V. Danilov, J. Lim, I. Moon, H. Chang, J. Power Sources 162 (2006) 992–1002.
[45] R. Chen, T. Zhao, J. Power Sources 152 (2005) 122–130.
[46] E. Kjeang, J. Goldak, M. Golriz, J. Gu, D. James, K. Kordesch, J. Power Sources 153 (2006) 89–99.
[47] W. Liu, C.-Y. Wang, J. Power Sources 164 (2007) 561–566.
[48] J. Ge, H. Liu, J. Power Sources 160 (2006) 413–421.
[49] H. Ju, C.-Y. Wang, J. Electrochem. Soc. 151 (2004) A1954–A1960.
[50] J. Norlund, G. Lindbergh, J. Electrochem. Soc. 149 (2002) A1107–A1113.
[51] K. Jeng, C. Chen, J. Power Sources 112 (2002) 367–375.
[52] T. Mennola, M. Noponen, M. Aroniemi, T. Hottinen, M. Mikkola, O. Himanen, P. Lund, J. Appl. Electrochem. 33 (2003) 979–987.
[53] T. Zhou, H. Liu, J. Power Sources 161 (2006) 444–453.
[54] M. Williams, E. Begg, L. Bonville, H. Kunz, J. Fentom, J. Electrochem. Soc. 151 (2004) A1173–A1180.
[55] R.B. Bird, W.E. Stewart, E.N. Lightfoot, Transport Phenomena, J. Wiley & Sons, New York, 1960.
[56] K. Scott, W. Taama, J. Cruickshank, J. Power Sources 65 (1997) 159–171.
[57] C.L. Yaws, Handbook of Transport Property Data: Viscosity, Thermal Conductivity and Diffusion Coefficients of Liquids and Gases, Gulf Pub Co., Houston, USA, 1995.
[58] E.N. Fuller, P.D. Schettler, J.C. Giddings, Ind. Eng. Chem. 58 (1966) 19–27.